IEEE Sensors Letters Volume 2(3) (2017)
Ultrasound Transducers

Characterization of Curved Piezoelectric Micromachined Ultrasound Transducers (pMUTs) Fabricated by Chip-Scale Glass Blowing Technique

Chichen Huang[1*], Shubham P. Khandare[2*], Sri-Rajasekhar Kothapalli[2], and Srinivas Tadigadapa[1]
[1] *Department of Electrical and Computer Engineering, Northeastern University, Boston, MA 02115, USA*
[2] *Department of Biomedical Engineering, The Pennsylvania State University, University Park, PA 16802, USA*

Received 1 Nov 2016, revised 25 Nov 2016, accepted 30 Nov 2016, published 5 Dec 2016, current version 15 Dec 2016. (Dates will be inserted by IEEE; "published" is the date the accepted preprint is posted on IEEE Xplore®; "current version" is the date the typeset version is posted on Xplore®).

Abstract—This paper presents the development of curved piezoelectric micromachined ultrasound transducers (pMUTs) using a novel chip-scale glass-blowing method on suspended glass templates. This new approach allows for controllable diaphragm curvature and high fill-factor arrays of varying sizes, making it possible to study the impact of the curvature on the performance of the pMUTs. A finite element analysis (FEA) model was built to guide the design. 30% Scandium doped Aluminum Nitride (Sc-AlN) was chosen for good piezoelectrical coefficient and biocompatibility. 100 nm platinum /750 nm Sc-AlN /100 nm gold films are sputtered on the curved glass membrane with diameters ranging from 75 μm to 750 μm. pMUT with diameter of 150 μm with 5.6 μm depth of curvature had resonance frequencies of 2.2 MHz along with center displacements up to 154 nm/V in air. Impedance measurements at resonance on the pMUTs show an k_{eff}^2 of 1.31%. Optimal curvatures were found experimentally and matched the FEA model. Changes in mode shapes were found when curvatures were deeper than optimal value.

Index Terms— Curved glass structures, Chip Scale Glassblowing, Aluminum Nitride, pMUT

I. INTRODUCTION

Ultrasound has been extensively used and investigated in medical applications such as medical imaging [1] and drug delivery [2] because of advantages like noninvasiveness, good penetration, good sensitivity, and ease of use. Prior to the development of pMUTs, conventional transducers were made of piezoelectric ceramics like lead zirconate titanate (PZT) [3]**.** These materials when operated in thickness mode exhibit a large impedance mismatch between the transducer surface and medium resulting in lower bandwidth unless augmented with one or more matching layers. With the development of MEMS technology, improvements in MUTs have been realized in several aspects such as wide bandwidth without the addition of matching layers [4], smaller cell size therefore higher operating frequency and better resolution, easier fabrication of large arrays at lower cost [5]. Despite lower electromechanical coupling coefficient, the low-power consumption feature makes pMUTs good candidates for a variety of applications, including intrabody communication [6], and fingerprint sensing [7].

To improve the maximum achievable electromechanical coupling in pMUTs, researchers are exploring novel geometry and boundary conditions. For example, Sammoura et al. have demonstrated a bimorph pMUT with dual electrodes that can improve the acoustic power per unit input voltage up to 400% [8]. pMUTs with suspended flexural membrane has been fabricated and has been shown to exhibit higher acoustic output than clamped pMUTs [9].

Recent studies suggest that curved pMUTs can generate high pressure output even for the small size of the membrane by leveraging in-plane stress as well as stress gradient in the pMUTs, as compared to planar pMUTs that use only stress-gradient in the stack for achieving out of plane bending [4, 10]. To realize curved pMUTs, fabrication methods used until now have mainly relied on isotropic etching of sacrificial silicon oxide and sealing the cavities in vacuum to realize templates for curved pMUTs [11, 12]. This process can yield very thin passive layer or even passive-layer-free pMUTs, but it inherently limits the design space in terms of pMUT diameters and achievable radius of curvature. Here we present an innovative chip-scale glass blowing process for realizing curved pMUTs without such constraints. Using this method, we were able to fabricate curved pMUTs with diameters varying from 75 μm to 750 μm with curvature depth ranging from 0.2 μm to76 μm.

II. DESIGN AND FABRIACATION

A. Simulation and Design

A 2D axisymmetric FEA model was created in COMSOL Multiphysics to study the effect of curvature. The material properties of Sc-AlN were used from [13]. In the simulation, the thickness of Sc-AlN was set as 750 nm and the thickness of glass was set as 2.75 μm. The radius of curvature was converted to a unitless value as 'curvature ratio' which is equal to radius of curvature divided by the normal radius of the cell. An eigenfrequency study was run first to estimate the resonance frequency in air. Then, a stationary study was done to estimate the static displacements. Finally, a Figure of merit (FOM) equal to the product of the fundamental resonance frequency and static displacement was calculated. This FOM can represent

Corresponding author: srinivas@northeastern.edu.
*Authors contributed equally to this paper.
Digital Object Identifier: 10.1109/LSEN.XXXX.XXXXXXX (inserted by IEEE).

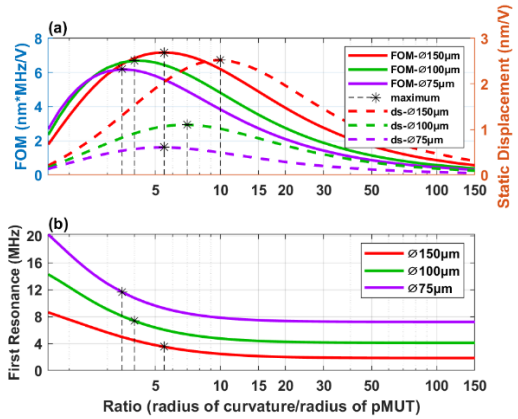

Fig. 1. (a) Simulated static displacement and FOM of curved pMUTs; (b) simulated first resonant of curved pMUTs. Ø is the PMUT diameter.

volumetric velocity which is proportional to acoustic pressure [10, 11, 14]. The simulated results are plotted in Fig.1 and will serve as the guidelines for designing curved pMUT.

As reported in [8], the performance of the curved pMUT increases as the ratio of the radius of curvature to radius of the pMUT increases reaching a maximum and thereafter decreases. This is because the higher curvature enables the transducer to convert more-effectively the in-plane strain into displacement but also increases the effective stiffness of structure. Thus, by tuning the curvature of a curved pMUT, we can increase the resonance frequency and displacement at the same time. However, the optimal ratio given by the FOM method is lower than the static displacement method, which means the device can potentially have a higher volumetric displacement output in spite of sacrificing the displacement sensitivity. The target ratio is between the two optimal values. For example, for 150 μm cells, the ratio should be between 6 and 10, corresponding to the curvature depth of 4 μm to 7 μm.

B. Fabrication Process

The three-mask surface micromachining process flow is shown in Fig. 2. A 500 μm thick silicon substrate was patterned with circles of various diameters ranging from 75 μm – 750 μm and etched to a depth of 250 μm using silicon DRIE. A 100 μm thick borosilicate glass (Schott Borofloat® 33) wafer was anodically bonded to the Si wafer in vacuum (10^{-4} Torr) to form vacuum-sealed cylindrical cavities. The bonded wafer was diced into chips and the glass layer was subsequently thinned down to 25 μm in 49% HF. Thereafter, the chips were placed on a ceramic heater. By controlling the temperature, time

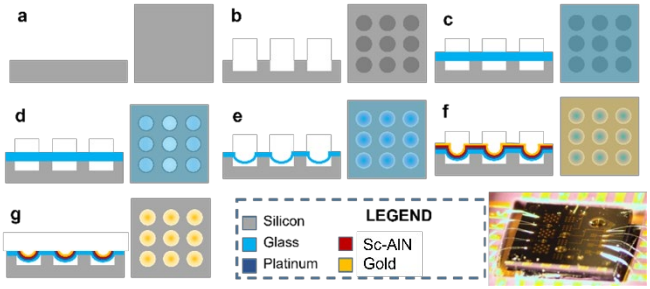

Fig. 2. Process flow of proposed pMUTs. (a)-(b) patterning and etching the Si substrate, (c) anodic bonding glass and Si, (d) glass etching, (e) glass blowing, (f) depositing Pt/Sc-AlN/Au, (g) patterning top electrode.

and thickness of glass, curved template surfaces of desired radius of curvature can be formed. The resulting curvature was measured with a profiler. The curved chips were etched again in HF to reduce the glass thickness to less than 4 μm to achieve the desired thickness of the passive template layer. Thereafter, 20 nm/100 nm Ti/Pt stack followed by 750 nm 30% Sc-AlN films were RF sputter deposited at a substrate temperature of 400 °C. Finally, 20 nm/100 nm thick Cr/Au layers were deposited and patterned with the 2nd mask by wet etching to form the top electrode. In the final step, the bottom Pt electrode was exposed by patterning and etching the Sc-AlN layer with the 3rd mask in an ICP-RIE tool.

C. Fabrication Results

An oblique view optical image of the fabricated device is also shown in Fig. 2. On the 5 mm square chip, there are 15 single element pMUTs with different diameters. Smaller circles are in the form of a small array, while larger circles are single devices. Due to the variations in the etched glass thickness from chip to chip, the depth of the curvature will be different from chip to chip for identical glass blowing conditions. For example, the 150 μm circles close to the edge of the chip have a curvature depth of 6.6 μm but only 1 μm for those at the center. For the smaller circles, the variation of curvature depth is less significant. However, these also need higher temperatures to reach the optimal curvature depth for the same glass thickness. The quality of the Sc-AlN film was verified using X-ray diffraction (XRD). Fig.3 shows the XRD scan and rocking curve obtained for the film deposited on one of the devices. The rocking curve resulted in a Full-Width Half-Maximum (FWHM) of 5.6°, which is much higher than the film on the dummy Si substrate from the same deposition which is around 2.8°. The reason for this was the poor roughness of the glass substrate after a deep HF etching. XRD measurements indicate mismatch in the crystalline orientation and are expected to degrade the piezoelectric coefficient.

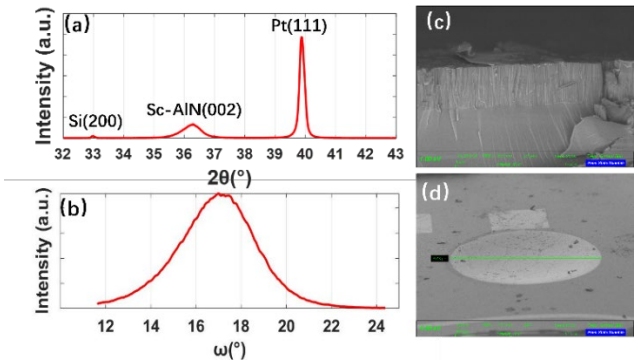

Fig. 3. (a) XRD measurement of the device. (b) Rocking curve at (002). (c) SEM image of the cross-section of the film. (d) Image of the 750 μm cell.

III. CHARACTERIZATION AND DISCUSSION

A. Characterization of smaller pMUTS

All elements were measured under a periodic chirp signal to find the resonance frequencies and corresponding modes using a Laser Doppler Vibrometer (LDV). Thereafter, each pMUT was excited by a sine signal at its resonant frequency to obtain the displacement. As

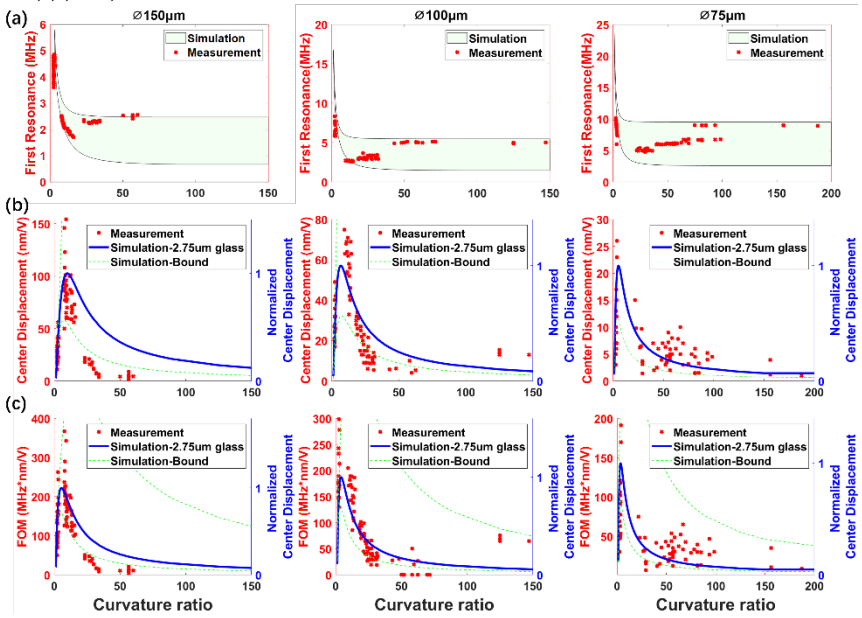

Fig. 4. (a) Resonance frequencies of all cells as a function of curvature to radius ratio for 150 μm, 100 μm, and 75 μm radius devices. (b) Center displacement of all cells as a function of the curvature to radius ratio. (c) FOM of all cells as a function of curvature to radius ratio

smaller pMUTs with diameters of 75 μm, 100 μm, and 150 μm were available in larger numbers, these were used for obtaining statistically better averaged performance metrics to study the trends. The measured results of smaller diameter pMUT are plotted in Fig. 4 along with the simulation results. The green band in Fig. 4(a) consists of the lower and upper bounds calculated when the glass thickness was 0.5 μm and 4 μm. Most data from the measurement falls inside this band; however, for smaller curvature to radius ratios, the measured resonance frequency is lower than the simulated results. Devices with higher curvature to radius ratio are closer to the upper bound because devices with thicker glass were less curved at the same temperature. In Fig. 4(b) and 4(c), the measured center displacements and FOM are plotted against the curvature to radius ratio of the pMUTs, respectively. Once again, the upper bound is simulated with 0.5 μm thick glass and the lower bound is with 4 μm thick glass; the blue curve is simulated with 2.75 μm thick glass. The measurement data shows the same trend as the simulation. An optimal ratio exists for a given diameter and this optimum will shift by the thickness of passive layer. For 150 μm pMUTs with optimal curvatures, most displacement amplitudes are between 60 nm/V and 100 nm/V; the largest displacement is 154 nm/V when the curvature depth is 5.6 μm and ratio is 9. Some pMUTs with less displacement have a higher FOM indicating that the output can potentially be improved by sacrificing the displacement sensitivity.

B. Characterization of larger pMUTs

Large single cell elements had a curvature that was much deeper than their optimum as these were glass blown on the same chips as the smaller ones. Six 275 μm diameter pMUTs with curvature ratio from 9.8 to 3.3 were tested. Fig.5 shows the average velocity of the scanned area and the mode shapes. In general, the modes are closer to each other than in a flat pMUT. Particularly, the (1,1) mode shifts closer to the (0,1) mode and eventually becomes the first mode detected by the LDV (Fig.5(e)). The (0,1) mode is not detectable either with LDV or the impedance analyzer. As shown in Fig.6, two types of (0,2) modes are observed and are called (0,2)a and (0,2)b here. (0,2)a has a

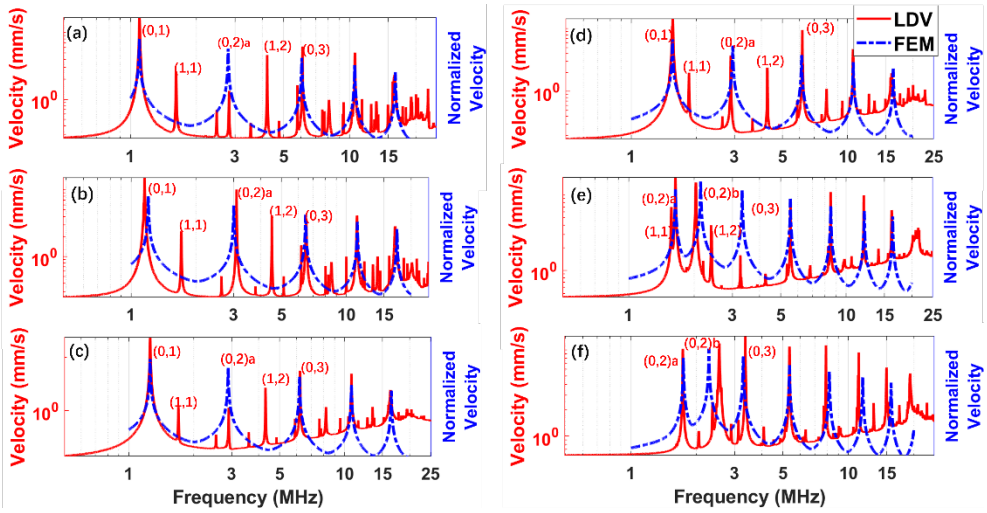

Fig. 5. (a-f) LDV measurements and FEM results of 275 μm cells of ratio=9.8, 8.7, 7.3, 5.6, 4.4, 3.3 respectively.

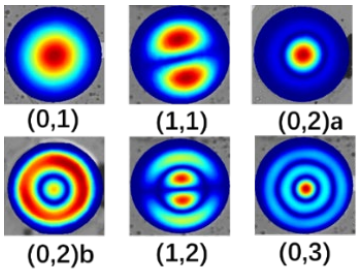

Fig. 6. Measured mode shapes.

stronger center deflection; however, for (0,2)b, the ring vibrates more intensely than the center. Fig. 7 shows the impedance measurement of the device in Fig.5(e). In Fig.7, the (0,2)b mode has the strongest resonance and a higher k_{eff}^2 of 1.49%.The results are also compared with FEA simulation in Fig. 5. It is found that the higher order resonances are barely affected by the curvature and mostly depend on the thickness of glass. But the first resonance is dependent on both parameters. By tuning the two parameters, the model can fit the measurement with minimum error. As discussed before, the pMUTs with deeper curvatures have a thinner glass and a higher coupling coefficient.

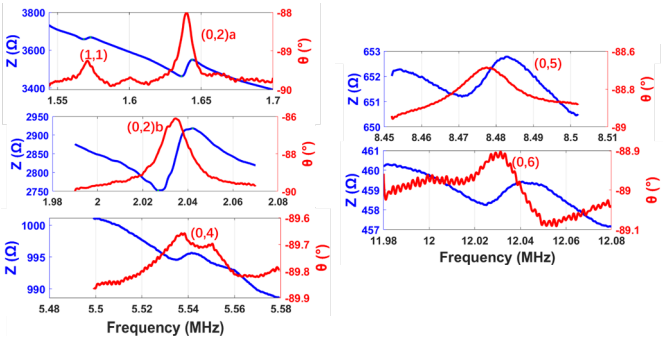

Fig. 7. Impedance measurements of the device in Fig. 5(e) corresponding modes are also identified in parenthesis.

LDV measurements were also performed on the device shown in Fig. 5(f) in oil under the same procedure to find the frequency response under load. Both Q factor and resonance frequency lowered due to the oil load. Interestingly, the (0,1) mode that was not measurable in air, appeared in the oil measurements. The bandwidth also improved significantly; all modes achieved a bandwidth larger than 4% and the (0,1) and (0,9) modes have a bandwidth over 10%. The stem chart in Fig. 8 shows the center displacement of the pMUT driven at (0,1) to (0,9) modes with 1 V sinusoidal signal. Although, having a lower displacement, the average velocity of the higher order modes of the pMUT outperform the first mode. Preliminary impulse

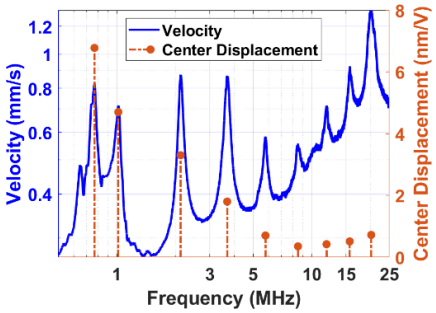

Fig. 8. LDV measurement of device in Fig. 5(e) under oil

responses obtained from the fabricated pMUTs revealed that the transducers could receive a wide range of frequencies (2.4 MHz to 4.7 MHz at -6 dB) and could likely improve image quality and resolution.

IV. CONCLUSION

In this work, curved pMUTs of different sizes and curvature depths were designed using a FEA model. The pMUTs with variouscurvature to radius ratio were fabricated using a novel glass-blowing technique. The fabricated devices were tested with LDV, and impedance analyzer and the results were compared with the simulation to study the role of curvature. The same trend was found in both the measurements and the simulations. An optimal curvature was obtained by using the Figure of Merit (FOM). The resonance frequency and displacement sensitivity of curved pMUTs were found to improve simultaneously as compared to flat pMUTs. Devices with different curvatures were tested in air and oil. It was found that, when the curvature is deep, mode shapes changed in air but not in oil. The higher order resonances showed improved performance for devices with deeper curvatures. Oil test was performed with selected devices and the bandwidth of all modes were seen to improve. Although, having a lower displacement, the average velocity of the higher order modes of the pMUT outperform the first mode. Finally, curvature reproducibility of the devices in future will be improved by placing same sized devices on a given chip, so that the glass blowing process results in identical curvatures across all devices. Furthermore, by polishing the glass prior to final thinning, we expect to realize a much smoother templating surface, which will allow for the deposition of better Sc-AlN films. These modifications are expected to further improve the performance of curved pMUTs.

V. REFERENCES

1. Feng, G.-H., et al., *Fabrication of MEMS ZnO dome-shaped-diaphragm transducers for high-frequency ultrasonic imaging.* Journal of Micromechanics and Microengineering, 2005. **15**(3): p. 586.
2. Mitragotri, S., *Healing sound: the use of ultrasound in drug delivery and other therapeutic applications.* Nature Reviews Drug Discovery, 2005. **4**(3): p. 255-260.
3. Desilets, C.S., J.D. Fraser, and G.S. Kino, *The design of efficient broad-band piezoelectric transducers.* IEEE Transactions on Sonics and Ultrasonics, 1978. **25**(3): p. 115-125.
4. Hajati, A., et al., *Three-dimensional micro electromechanical system piezoelectric ultrasound transducer.* Applied Physics Letters, 2012. **101**(25): p. -.
5. Oralkan, O., et al., *Capacitive micromachined ultrasonic transducers: next-generation arrays for acoustic imaging?* IEEE Transactions on Ultrasonics, Ferroelectrics, and Frequency Control, 2002. **49**(11): p. 1596-1610.
6. Pop, F., B. Herrera, and M. Rinaldi, *Lithium Niobate Piezoelectric Micromachined Ultrasonic Transducers for high data-rate intrabody communication.* Nature Communications, 2022. **13**(1): p. 1782.
7. Jiang, X., et al. *Monolithic 591×438 DPI ultrasonic fingerprint sensor*. in *2016 IEEE 29th International Conference on Micro Electro Mechanical Systems (MEMS)*. 2016.
8. Akhbari, S., et al. *Bimorph pMUT with dual electrodes*. in *2015 28th IEEE International Conference on Micro Electro Mechanical Systems (MEMS)*. 2015.
9. Guedes, A., et al. *Aluminum nitride pMUT based on a flexurally-suspended membrane*. in *2011 16th International Solid-State Sensors, Actuators and Microsystems Conference*. 2011.
10. Akhbari, S., et al. *Highly responsive curved aluminum nitride pMUT*. in *2014 IEEE 27th International Conference on Micro Electro Mechanical Systems (MEMS)*. 2014.
11. Wu, S., et al. *An Aluminum-Nitride PMUT with Pre-Concaved Membrane for Large Deformation and High Quality-Factor Performance*. in *2021 21st International Conference on Solid-State Sensors, Actuators and Microsystems (Transducers)*. 2021.
12. Calame, F. and P. Muralt, *Novel 3D PZT thin film structure for micromechanics.* Journal of Electroceramics, 2007. **19**(4): p. 399-402.
13. Urban, D.F., O. Ambacher, and C. Elsässer, *First-principles calculation of electroacoustic properties of wurtzite (Al,Sc)N.* Physical Review B, 2021. **103**(11): p. 115204.
14. Jiang, X., et al. *Improving PMUT Transmit Performance via Sub-Micron Thickness Scaling*. in *2018 IEEE International Ultrasonics Symposium (IUS)*. 2018.